SPECIAL TOPICS

Nonlinear gyrokinetic simulations of reversed shear Alfven eigenmodes in DIII-D tokamak

P. Liu[1] · X. Wei[1] · Z. Lin[1] · G. Brochard[1,2] · G. J. Choi[1] · J. H. Nicolau[1]

Abstract

Global gyrokinetic simulations of reversed shear Alfven eigenmodes (RSAE) excited by energetic particles (EP) in the DIII-D discharge #159,243 find that self-generated zonal flows dominate the RSAE nonlinear saturation. Effects of Coulomb collisions are negligible since the effective EP collision frequency is much smaller than the RSAE linear growth rate. Nonlinear interactions of multiple unstable RSAEs lower the saturation amplitude and resulting EP transport, and nonlinearly generate toroidal Alfven eigenmodes (TAE) and ellipticity induced Alfven eigenmodes (EAE). In both single mode and multiple modes simulations, the initial RSAE saturation amplitude and associated EP transport are an order of magnitude higher than the experimental observations, but quickly diminish within 0.1 ms after nonlinear saturation due to the formation of coherent phase space structures that flatten the EP distribution function at resonances. Results from these simulations of the RSAE only show that additional dissipation such as background micro-turbulence is needed to sustain the quasi-steady state RSAE amplitude and EP transport observed in this DIII-D experiment.

1 Introduction

Confinement of energetic particles (EP) (Fasoli et al. 2007; Breizman and Sharapov 2011; Lauber 2013; Gorelenkov et al. 2014; Todo 2019; Heidbrink and White 2020), including both fusion products (α particles) and fast ions produced by auxiliary heating through ion cyclotron radio frequencies (ICRF) waves or neutral beams

---

✉ P. Liu
   pengfl8@uci.edu

1   Department of Physics and Astronomy, University of California, Irvine, CA 92697, USA

2   Present Address: ITER organisation, Route de Vinon de Verdon, CS 90 046 13067, Saint-Paul Lez Durance, France

injection (NBI), determines the performance of current and future fusion reactors. Meso-scale Alfven Eigenmodes (AE) (Heidbrink 2008; Chen and Zonca 2016), driven by strong EP pressure gradients, can cause an anomalous EP transport in the core region that reduces the heating efficiency. The AE turbulence and associated EP transport, thus, have drawn intense experimental and theoretical research.

Thanks to the rapid growth of computational power, numerical simulations of AE and EP physics play an increasingly more important role in the explanation and prediction of EP confinement in the last two decades. Early kinetic-MHD simulation efforts to understand the nonlinear AE evolution focus on nonlinear wave particle interaction leading to mode saturation, frequency chirping, and fast ion loss (Spong et al. 1994; Fu and Park 1995; Pinches et al. 1998; Todo et al. 2003). The types of nonlinear frequency chirping are found to be dependent on the EP drive and the mode damping in kinetic-MHD simulations (Wang et al. 2021). Beyond the conventional paradigm of a 1D nonlinear dynamical system for the wave particle interaction, nonlinear gyrokinetic simulations (Zhang et al. 2012) find a fast (i.e., non-adiabatic) oscillation of AE frequency and amplitude due to the intrinsically 2D nonlinear dynamical system, where the radial variations of mode amplitude induce resonance detuning and radial decoupling in the evolution of coherent structures in phase space (Zonca et al. 2015). Both hybrid and gyrokinetic simulations (Lang et al. 2010; Chen et al. 2013) find that Coulomb collisions of EP increase the AE saturation level due to the destruction of coherent structures (Berk et al. 1992). Nonlinear MHD effects and zonal flows are first found to be not important for weakly unstable mode near marginality in kinetic-MHD simulations (Todo et al. 2010). Subsequent nonlinear gyrokinetic simulations (Chen et al. 2018) find that the RSAE saturation amplitude is reduced by the self-generated $n = 0$ component in the electron density and thermal ion distribution (zonal structures) when $\gamma/\omega \geq 3\%$ (γ is AE linear growth rate and ω is AE frequency), which indicates the strength of the RSAE instability when the dominant mechanism for the RSAE saturation changes from nonlinear wave particle trapping near marginality to zonal structure effects far away from marginality. Furthermore, a systematic comparison between single mode and multiple mode AE has been reported in kinetic-MHD simulations (Vlad et al. 2018), while the $n = 0$ component is not considered. Recently, verification and validation studies of AE (Spong et al. 2012; Taimourzadeh et al. 2019) have been carried out. Moreover, a full comparison of nonlinear results has been reported between gyrokinetic and hybrid codes (Cole et al. 2017). Nonetheless, nonlinear physics of AE has not been fully understood regarding the role of zonal flows, multiple mode interactions, and cross-scale couplings with realistic parameters.

Furthermore, the AE turbulence and EP transport may depend on nonlinear cross-scale coupling with micro-turbulence (Horton 1999; Heidbrink et al. 2009) and macro-scale MHD instabilities. In this work, we study both AE nonlinear physics and cross-scale coupling through integrated simulations using the global gyrokinetic toroidal code GTC (Lin et al. 1998). Recent GTC simulations coupling micro–meso-scales find the regulation of RSAE by ion temperature gradient (ITG) micro-turbulence (Liu et al. 2022). In the presence of the background micro-turbulence, RSAE amplitude and EP transport decrease drastically at the initial saturation but subsequently increase to the experimental levels in the quasi-steady state with

burst dynamics, due to the scattering of nonlinearly trapped EP and the damping of zonal structures by the micro-turbulence. The RSAE amplitude in the quasi-steady-state ITG-RSAE turbulence from gyrokinetic simulations, for the first time, agrees very well with experimental observations.

As a follow-up to Liu et al. (2022), we report here the detailed nonlinear physics of the AE turbulence regarding the role zonal flows and multiple mode interactions from GTC simulations of the RSAE only. The detailed physics of the cross-scale coupling between RSAE and micro-turbulence will be reported in a future paper. The simulated DIII-D discharge #159,243 has been selected as the reference case for verification and validation (V&V) of linear gyrokinetic simulations (Taimour-zadeh et al. 2019). RSAEs are found to be excited by beam ions near the q_{min} flux surface using eight simulation codes (including gyrokineticLin et al. 1998; Candy and Waltz 2003; Chen and Parker 2003; Jolliet et al. 2007; Mishchenko et al. 2014), gyrokinetic-MHD hybrid (Todo and Sato 1998; Varela et al. 2017), and eigenvalue (Cheng and Chance 1986) codes) with good agreement on both real frequency and linear growth rate. Poloidal contour plot and radial mode structures of the $n = 4$ RSAE also agree with the electron cyclotron emission (ECE) (Austin and Lohr 2003) and electron cyclotron emission imaging (ECEI) (Tobias et al. 2010) measurements. Subsequent linear global GTC simulations (Wang et al. 2021) find that RSAE are unstable including the most unstable modes with toroidal mode number $n = (4, 5)$, less unstable modes $n = (3, 6, 7, 8)$, and marginally unstable modes $n = [9, 12]$. Compressible magnetic perturbation slightly increases the RSAE linear growth rate, while effects of trapped electrons on the linear dispersion relation are insignificant.

Building on the comprehensive linear simulations, we perform nonlinear gyro-kinetic simulations to study RSAE saturation and EP transport. We examine the effects of zonal flows, collisions of beam ions, and nonlinear toroidal mode coupling on the RSAE amplitude and the associated EP transport. In single toroidal mode simulations, self-generated zonal flows strongly affect both RSAE amplitude and EP transport for the most unstable modes. Effects of Coulomb collisions of beam ions are found to be negligible since the effective collision frequency of beam ions is much smaller than linear growth rate of the RSAE.

In multiple toroidal modes simulation, the most unstable mode saturates at lower amplitude, while the stable and marginally unstable modes can be nonlinearly generated by toroidal mode coupling between strongly unstable modes. In the multiple mode simulation, toroidicity-induced Alfven eigenmode (TAE) and ellipticity induced Alfven eigenmode (EAE) could be nonlinearly generated outside the q_{min} flux surface after RSAE nonlinear saturation.

In global simulations of both single mode and multiple modes, RSAE mode amplitude and associated EP transport are an order of magnitude higher than the experimental observations (Collins et al. 2016; Heidbrink et al. 2017) at the nonlinear saturation, but quickly diminished within 0.1 ms after nonlinear saturation due to the flattening of EP distribution function at resonances. No steady state can be obtained in the absence of additional dissipation or background micro-turbulence in the simulations of this DIII-D experiment where only a few toroidal modes are unstable (Zonca et al. 2015; Liu et al. 2022; Bass and Waltz 2010; Duarte et al.

2017; Zeeland et al. 2019; Gorelenkov and Duarte 2021; Biancalani et al. 2021). These GTC simulation results show that the perfect equilibrium (i.e., without ubiquitous background micro-turbulence) as the initial condition for the RSAE simulation can lead to the excessive overshoots of the RSAE amplitude in the nonlinear saturation and the diminished EP transport immediately after the nonlinear saturation. Such a perfect initial condition has been used in nearly all plasma simulations, but nonetheless is not realistic. In fact, Liu et al. (2022) shows that the presence of the micro-turbulence as the background for the RSAE simulation can greatly reduce the RSAE initial nonlinear saturation amplitude and maintain a quasi-steady state EP transport consistent with experimental observations.

This paper is organized as follows: The equilibrium profiles and simulation parameters are described in Sect. 2. In Sect. 3, we present the simulation results of single mode simulations and discuss the zonal flow effects and phase space dynamics. In Sect. 4, we discuss EP collisional effects on the RSAE nonlinear dynamics. In Sect. 5, we present the simulation results of multiple mode interactions. Finally, conclusions and discussion are presented in Sect. 6.

2 Equilibrium profiles and simulation parameters

In this work, the kinetic EFIT magnetic equilibrium geometry and plasma profiles including the classical fast ion density as shown in Figs. 2 and 3 of Taimourzadeh et al. (2019) are selected from DIII-D shot # 159,243 at 805ms. The safety factor q profile has a reversed shear with minimal value $q_{min} = 2.94$ near $\rho = 0.5$, where RSAE can be excited by beam ions. Here, ρ is square root of toroidal flux normalized by its separatrix value.

GTC (Lin et al. 1998) used in this work is a global toroidal code using gyrokinetic (Brizard and Hahm 2007) ions and drift-kinetic electrons, which has been applied to driftwave micro-turbulence (Lin et al. 1998, 2002; Zhang et al. 2008; Xiao and Lin 2009; Wang et al. 2020; Nicolau et al. 2021), magnetohydrodynamic (MHD) instabilities (McClenaghan et al. 2014; Brochard et al. 2022) and AE (Deng et al. 2012a , 2012; Wang et al. 2013; Choi et al. 2021). In this paper, all species (EP, thermal ions and electrons) are treated on the same footing using the low noise δf scheme (Parker and Lee 1993). Compressible magnetic perturbation $\delta B_{\parallel}$ (Dong et al. 2017) and equilibrium current (Deng et al. 2012b) are incorporated for a physically comprehensive simulation. The electron response is further expanded using the fluid-kinetic hybrid model (Deng et al. 2012b). Global equilibrium pressure profiles of each species are fixed using a model particle and heat source. We have verified that fixing the global profiles, which has been routinely applied in the global gyrokinetic simulations of the micro-turbulence to prevent profile relaxation (Lin et al. 2002), does not change the nonlinear RSAE physics including the role of zonal flows in the RSAE saturation and nonlinear evolution of RSAE mode amplitude and EP transport. Time step is set to be $10^{-8}s$ to resolve the high-frequency EAE (142kHz) and to resolve the electron orbital frequency as well as the frequency of unphysically high $k_{\parallel}$ Alfven wave for numerical stability. GTC uses a global field-aligned mesh with 32 parallel grids which are sufficient because of

the long parallel wavelength. In the nonlinear electromagnetic simulations of single toroidal mode RSAE, based on the convergence studies, 5×10^4 unstructured perpendicular grids with grid size $\sim 1.3\rho_i$ and 1000 particles per cell for each species with a local Maxwellian are used, where $\rho_i \sim 2.1mm$ is the thermal ion gyroradius. In the simulation of multiple modes RSAE, however, a larger marker number and denser mesh are used to reduce the noise and to provide a better spatial resolution, where 2×10^5 unstructured perpendicular grids and 6000 particles per cell for each species are used. In all simulations, all poloidal m harmonics are kept when using Fourier filtering to select specific toroidal modes.

3 Nonlinear simulations of a single toroidal mode

3.1 Effects of zonal flows on RSAE saturation

Nonlinear simulations of a single mode RSAE for the most unstable mode $n = 4$, less unstable mode $n = 6$, and marginal unstable mode $n = 10$ are performed to investigate the effects of zonal flows on the RSAE nonlinear saturation. Figure 1 shows the time evolution of the normalized electrostatic potential $e\delta\phi/T_e$ (here, e is electron charge) on the q_{min} flux surface from simulations self-consistently keeping zonal flows or artificially suppressing zonal flows. For the most unstable mode $n = 4$ with a linear growth rate γ of $\gamma_4/\omega_4 \sim 8\%$ (here ω_4 is the real frequency) shown in Fig. 1a, the RSAE saturates at a very high level with an electrostatic potential $\delta\phi \sim T_e/e$ but quickly drops by a factor of more than 20 to a very low level within $0.2ms$ when zonal flows are suppressed in the simulations. In the simulation keeping zonal flows, zonal flows are generated by mode coupling with a nonlinear growth rate $\gamma_0 \sim 2\gamma_4$. Zonal flows, in turn, reduce the mode saturation amplitude by a factor of more than 2. After nonlinear saturation, the mode amplitude also quickly drops to a very low level. For the less unstable mode $n = 6$ with $\gamma_6/\omega_6 \sim 5\%$ as shown in Fig. 1b, zonal flows also play an important role in the RSAE saturation, and the saturation amplitude is smaller than that of $n = 4$ RSAE. However, for marginally unstable mode $n = 10$ with $\gamma_{10}/\omega_{10} \sim 2\%$ as shown in Fig. 1c, the effects of zonal flows are insignificant, and the mode saturate at very low amplitudes. These results are consistent with previous GEM simulations (Chen et al. 2018) of the $n = 4$ RSAE using the same DIII-D equilibrium but scanning fast ion density, which found that the effects of zonal structures are insignificant for weakly unstable mode $\gamma/\omega \leq 3\%$.

The mode structures of the $n = 4$ RSAE from simulations with zonal flows are in Fig. 2 from the linear phase [panel (a)] to the nonlinear saturation [panel (b)] and late nonlinear stage [panel (c)]. The corresponding radial profiles of each poloidal harmonics are shown in Fig. 3. Besides the dominant harmonic $m = 12$, there are two subdominant harmonics $m = 11$ and $m = 13$. In the linear phase, the mode peaks at the q_{min} flux surface and exhibits triangular shape with a wide radial structure. At the nonlinear saturation as shown in Fig. 2b, besides the dominant peak at the q_{min} surface, another peak appears inside the q_{min} surface. Away from the q_{min} flux surface, the outer part of RSAE mode structure, which is subdominant but still visible in the linear phase, exhibits ballooning structure and

Fig. 1 Time history of perturbed electrostatic potentials $e\delta\phi/T_e$ on the q_{min} flux surface from single mode simulations of $n = 4$ [panel (**a**)] with (green) or without (red) zonal flows (black). Time histories of $e\delta\phi/T_e$ from single mode simulations of $n = 6$ and 10 are shown in panels (**b**) and (**c**)
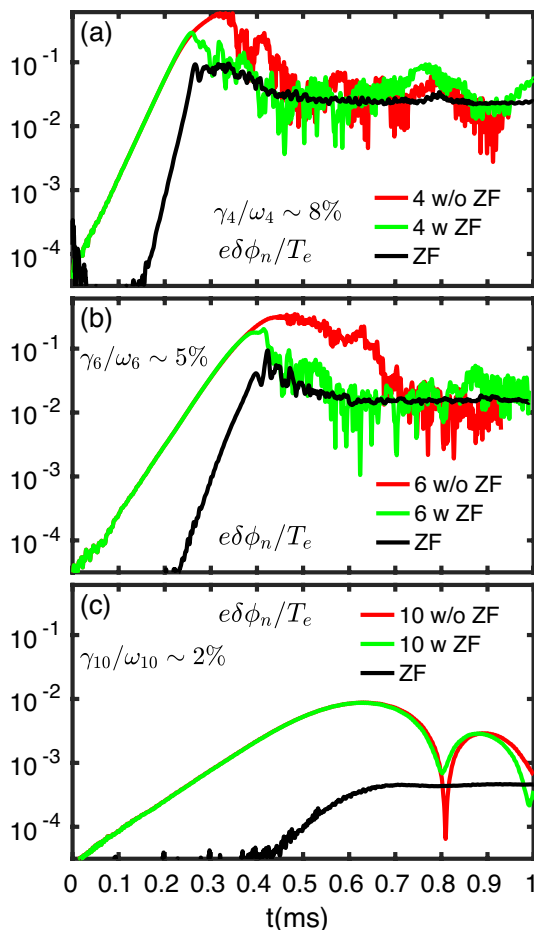

saturates at a level of about 25% of the main peak's amplitude near q_{min} surface. And the corresponding radial structures show coupling of different poloidal harmonics in the major radial domain $R = [2.05, 2.2]m$ due to strong magnetic shear. But it is not TAE since no clear TAE frequency is found at the RSAE saturation. At the late nonlinear stage, besides the decrease of the mode amplitude compared with that at the nonlinear saturation, the mode amplitude near q_{min} as shown in Fig. 3c, is suppressed after initial nonlinear saturation due to zonal flows and flattening of resonant EP distribution in phase space.

The instantaneous frequencies of electrostatic potential $e\delta\phi/T_e$ of $m = 12$ harmonic and zonal flows near the q_{min} flux surface are shown in Fig. 4. In linear phase, $m = 12$ harmonic grows exponentially with the linear frequency, and zonal flows grow with a zero frequency. After nonlinear saturation, the frequency of $m = 12$ harmonic exhibits up and down chirping in the nonlinear phase. For the
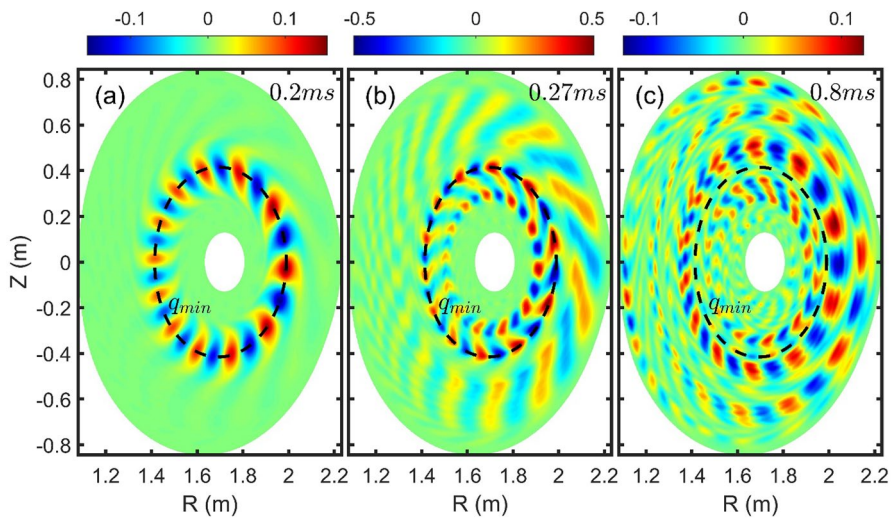
Fig. 2 Poloidal contour plots of perturbed electrostatic potential $e\delta\phi/T_e$ in linear phase [panel (**a**)], nonlinear saturation [panel (**b**)] and late nonlinear stage [panel (**c**)] from single mode simulation of $n = 4$ with zonal flows
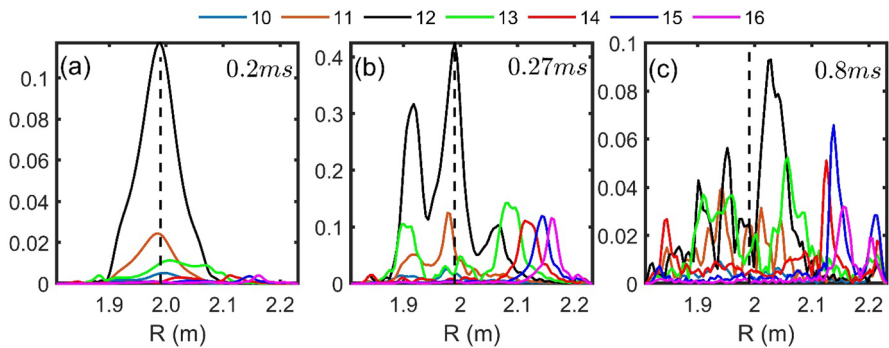

Fig. 3 Radial profiles of poloidal harmonics in linear phase [panel (**a**)], nonlinear saturation [panel (**b**)] and late nonlinear stage [panel (**c**)] from single mode simulation of $n = 4$ with zonal flows

zonal flows, however, GAM oscillation $\sim 40kHz$ together with their second and third harmonics appears in the nonlinear phase.

The time evolution of the resulting effective EP diffusivity $D_f(t)$ driven by the most unstable RSAE $n = 4$ is shown in Fig. 5. Here, $D_f(t)$ are obtained by averaging over the major radial domain $R = [1.95, 2.04]m$ of fast ion diffusivity $D_f(R, t)$ as function of major radius R and time t,
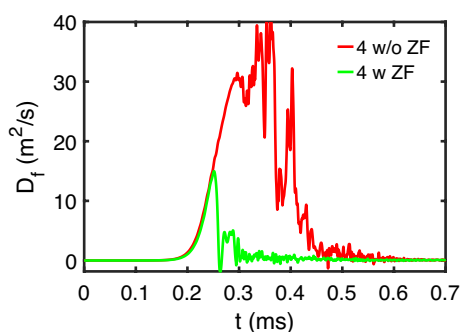
$$D_f(R, t) = \int v_{dr}(R, t)\delta f(R, t)dv^3/\nabla n_f,$$

Fig. 4 Frequency spectrum evolution of perturbed electrostatic potential $e\delta\phi/T_e$ of $m = 12$ harmonic [panel (**a**)] and zonal flows [panel(**b**)] near the q_{min} flux surface from single mode simulation of $n = 4$ with zonal flows
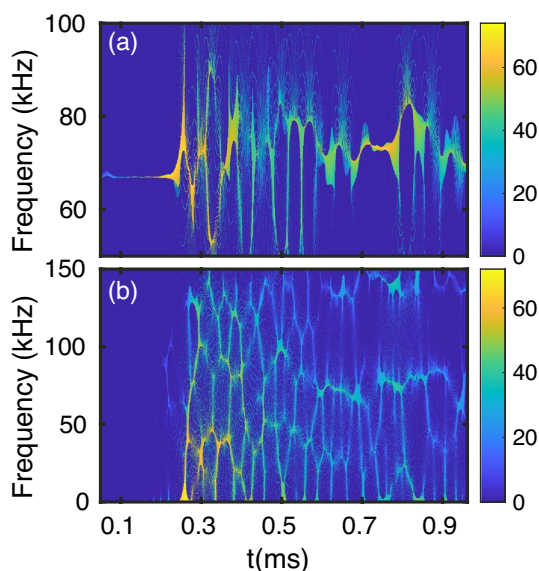
Fig. 5 Time history of averaged effective fast ion diffusivity of single mode simulations of $n = 4$ with (green) and without (red) zonal flows

where v_{dr} is the radial component of gyrocenter drift velocity $\boldsymbol{v}_d$ including $\boldsymbol{E} \times \boldsymbol{B}$ drift and magnetic-flutter term,

$$\boldsymbol{v}_d = \frac{c\boldsymbol{B}_0 \times \nabla\langle\delta\phi\rangle}{B_0^2} + v_{||}\frac{\delta\boldsymbol{B}_\perp}{B_0}$$

with gyro-averaging $<>$, δf is the perturbed beam ion distribution function, and n_f is the equilibrium beam ion density. Without zonal flows, the averaged EP diffusivity reaches $40m^2/s$ at the RSAE saturation, but drops to a very low level $D_f \ll 1m^2/s$ within $0.2ms$. When zonal flows are kept, the averaged EP diffusivity is reduced to $15m^2/s$ by zonal flows near the RSAE saturation, which is still much larger than experimental value of EP diffusivity. It also quickly drops to almost 0 in $0.1ms$ after the nonlinear saturation, which is inconsistent with the quasi-steady state EP transport observed in the experiment.

3.2 Phase space dynamics

Despite the differences in the saturation amplitudes among various unstable RSAE, a common phenomenon is that all mode amplitudes drop quickly to a very low level after the nonlinear saturation, presumably due to the formation of coherent phase space structures. The dynamics of EP phase space coherent structures associated with the precessional resonance with the beta-induced Alfven eigenmodes (BAE) (Zhang et al. 2012, 2013; Cheng et al. 2017) has been studied previously by GTC simulations and illustrated in the phase space of canonical variables $\left(\zeta, P_\zeta\right)$, where ζ is toroidal angle and P_ζ is the canonical angular momentum,

$$P_\zeta = g \frac{m_f}{Z_f B_0} v_{f\|} - \psi,$$

with g the covariant component of equilibrium magnetic field, B_0 the equilibrium magnetic field, ψ the poloidal magnetic flux function, and m_f, Z_f, $v_{f\|}$ the beam ion mass, charge, and parallel velocity, respectively. For the precessional resonance, the magnetic moment μ and longitudinal invariant $J_\|$ are constants, and the nonlinear dynamics of the gyrocenters is reduced to one degree of freedom described by the pair of action-angle variables $\left(\zeta, P_\zeta\right)$.

In the current simulations, the dominant resonances responsible for the RSAE excitation have been identified by analyzing EP phase space structures shown in Fig. 6. In the axisymmetric tokamaks, the resonant condition of Alfven eigenmodes is $\omega - n\omega_p - \left(l + n\bar{q} - m\right)\omega_b = 0$ for passing particles, and $\omega - n\omega_p - l\omega_b = 0$ for trapped particles, where l is an integer number, $\bar{q} = \oint q d\theta / \oint d\theta$ with the poloidal angle θ, $\omega_b = 2\pi \left(\oint d\theta / \dot{\theta}\right)^{-1}$ is the transit/bounce frequency for passing/trapped particles, and $\omega_p = (2\pi)^{-1} \omega_b \oint \left(\dot{\zeta} - q\dot{\theta}\right) d\theta / \dot{\theta}$ is the precessional frequency (Zonca and Chen 2014), respectively. The relative strength of resonances can be inferred from the intensity of fast ion entropy δf^2 in the phase space using constants of motions of linear orbits (E, λ), where E is the kinetic energy and $\lambda = \mu B_a/E$ is the pitch angle with on-axis equilibrium magnetic field B_a. The trap-passing boundary at q_{min} surface is roughly $\lambda = 1 - r_0/R_0$, where $r_0 = 0.158 R_0$ is the distance from the radial location of q_{min} at outer midplane to the magnetic axis with the on-axis major radius $R_0 = 1.732m$. In Fig. 6, the colored lines represent various resonances of trapped particles estimated from analytic model (White 2006) using the local

Fig. 6 Phase space (E, λ) structures of δf^2 in linear phase from single mode ($n=4$) simulation with zonal flows. The colored lines are dominant resonances. Here $\omega_d = 4\omega_p$
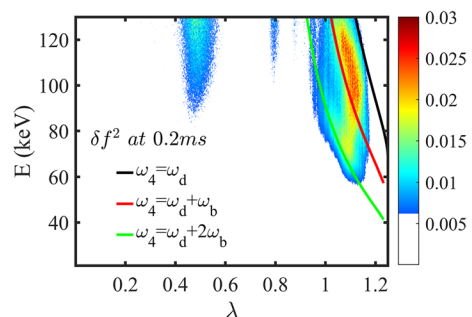
parameters on the q_{min} flux surface. The resonances appear to be very complicated because of multiple resonances mostly contributed by trapped particles. The dominant resonances are drift bounce resonances $\omega_4 = \omega_d + \omega_b$ and $\omega_4 = \omega_d + 2\omega_b$ in both linear and nonlinear phases.

The amplitudes of the two frequencies (ω_d and ω_b) along the linear resonance lines appear to be comparable as shown in Fig. 7, i.e., there is no time scale separation between the bounce and precessional motion. Therefore, the nonlinear EP dynamics have intrinsically two-degree of freedom and need to be described in the phase space defined by two pairs of action-angle variables (ζ, P_ζ) and $(\theta, J_{\parallel})$. This 2D dynamics may be responsible for the lack of a simple clump-hole pair across the resonance lines, contrary to that expected by the analytic model (Berk et al. 1992; Hezaveh et al. 2022) based on the 1D nonlinear wave particle interaction.

Despite the intrinsic two-degree of freedom, the dynamics system still preserves the magnetic moment μ. We now choose some values of μ and analyze the nonlinear evolution of δf in the phase space using the remaining two constants of motion (P_ζ, λ). Here, we focus on the $n = 4$ RSAE with zonal flows. We first choose a magnetic moment of $\mu B_a = 80 keV$ to examine the nonlinear dynamics of dominant resonant particles, trapped particles. The phase space structures are present in Fig. 8 from linear phase in panel (a) to nonlinear saturation in panel (b) and late nonlinear stage in panel (c) and panel(d), where P_ζ is normalized by the poloidal magnetic flux function on the wall ψ_w. Selecting the maximal δf^2 along P_ζ in Fig. 8a, the black line represents the dominant resonance in the linear phase. In the nonlinear phase, the clump–hole pairs form across the resonance line, where the red regions represent the positive value and blue regions represent the negative value. The phase space structures peak at $(-0.2, 1.1)$ in (P_ζ, λ) phase space, which means the dominant resonant particles are deeply trapped particles with $l=1$ (Brochard et al. 2020) near q_{min} surface. Near the nonlinear saturation, the structures broaden along the resonance line and extend in energy

Fig. 7 Dependence of precessional and bounce frequencies on EP energy E along RSAE resonance lines in Fig. 6 for drift bounce resonances $\omega_4 = \omega_d + \omega_b$ [panel (**a**)] and $\omega_4 = \omega_d + 2\omega_b$ [panel (**b**)]
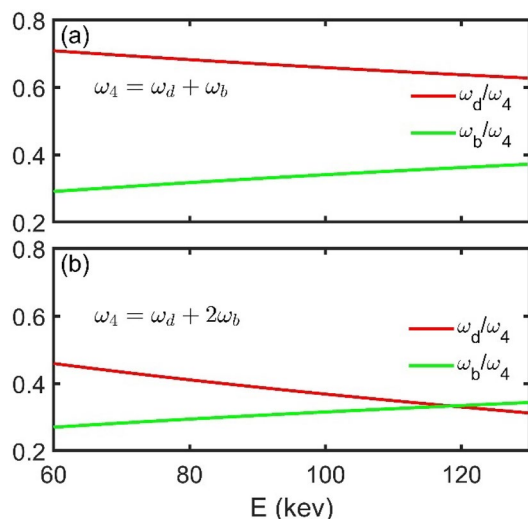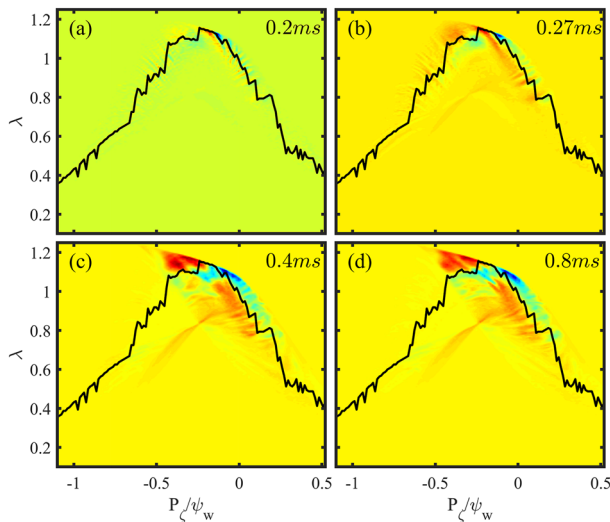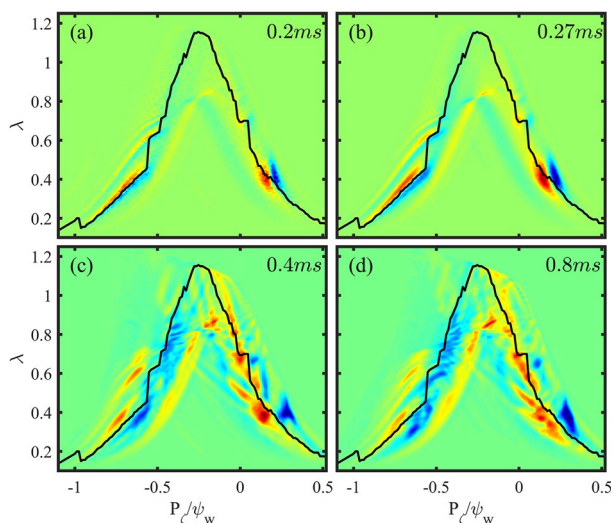
Fig. 8 Perturbed beam ion distribution function δf in (P_ζ, λ) phase space at 0.2ms [panel (**a**)], 0.27ms [panel (**b**)], 0.4ms [panel (**c**)], and 0.8ms [panel **d**] from single mode ($n=4$) simulation with zonal flows for a magnetic moment $\mu B_a = 80 keV$. The black line represents the dominant resonance

and radial directions. This may explain the radial extension of the mode structure as shown in Fig. 2b. After nonlinear saturation, the structures extend perpendicular to the resonance line and the co-passing resonant particles with $l = -7$ near trapped-passing boundary $(P_\zeta, \lambda) = (0.1, 0.89)$ also play important role, as shown in Fig. 8c. The clump–hole pairs lead to the flattening of EP profile, which reduces the drive of EP distribution function and the RSAE mode amplitude. From 0.4ms to 0.8ms, the phase space structures barely change. As a result, the RSAE mode amplitude persists a lower level and never increases again. Moreover, two dominant negative regions which separated by the positive region near $(P_\zeta, \lambda) = (-0.2, 1.1)$ in linear phase and nonlinear saturation merge to form one large negative structure after 0.4ms. The gradient of EP distribution function perpendicular to the resonance line decreases to almost 0 from linear to nonlinear phase.

We then choose a magnetic moment of $\mu B_a = 25 keV$ to examine the phase space structure contributed by both passing and trapped particles. The phase space structures are plotted in Fig. 9 from linear phase in panel (a) to nonlinear saturation in panel (b) and late nonlinear stage in panel (c) and panel(d). In the linear phase, the dominant resonant particles are passing particles, where the left dominant structure is contributed by counter-passing particles with $l = 14$ near $(P_\zeta, \lambda) = (-0.66, 0.38)$ and right one by co-passing particles with $l = 10$ near $(P_\zeta, \lambda) = (0.2, 0.4)$. Near the nonlinear saturation, passing particles still dominate the resonance, as shown in Fig. 9b. After nonlinear saturation, trapped particles also play important role. Again, the flattened EP profile reduces the drive of EP distribution perturbation and RSAE mode amplitude.

Fig. 9 Perturbed beam ion distribution function δf in (P_ζ, λ) phase space at 0.2ms [panel (**a**)], 0.27ms [panel (**b**)], 0.4ms [panel (**c**)], and 0.8ms [panel (**d**)] from single mode ($n=4$) simulation with zonal flows for a magnetic moment $\mu B_a = 25keV$. The black line represents the dominant resonance

4 Collisional effects on the RSAE nonlinear dynamics

We now perform nonlinear simulations of the most unstable n=4 RSAE to study effects of Coulomb collisions, which can destroy the EP coherent phase space structures. The effects of collisions on the RSAE amplitude and EP transport level depend on the ratio of the RSAE growth rate and effective collision frequencies. The slowing down rate of beam ions is $\nu_{fe}^\epsilon = 19s^{-1}$ due to thermal electrons and $\nu_{fi}^\epsilon = 26s^{-1}$ due to thermal ions, and the pitch angle scattering rate due to thermal ions is $\nu_{fi}^{scatt} = 21s^{-1}$ for plasma parameters near q_{min} flux surface, i.e., electron density $n_e = 3.1 \times 10^{13} cm^{-3}$, beam ion density $n_f = 1.95 \times 10^{12} cm^{-3}$, electron temperature $T_e = 850eV$, thermal ion temperature $T_i = 935eV$, beam ion temperature $T_f = 20keV$, and effective charge $Z_{eff} = 1.66$. The effective collision frequency (Hinton and Hazeltine 1976) is much larger than the collision frequency for the process of collisional diffusion across the small phase space structure associated with the sharp resonance due to the fact that the RSAE $\gamma/\omega \ll 1$.

To compare with earlier RSAE simulations (Lang et al. 2010; Chen et al. 2013), we first study collisional effects in GTC simulations without zonal flows by including pitch angle scattering of the EP due to thermal ions. GTC simulations find that collisional effects on both RSAE saturation amplitude and associated fast ion diffusivity are insignificant when using realistic collision frequency. When we use a collision frequency 10 times or 100 times of the realistic frequency, collisional effects enhances both RSAE saturation amplitude and associated EP diffusivity, but the effects are still very weak at the late nonlinear stage as shown in Fig. 10(a). If the collision frequency is further amplified to 1000 times, a quasi-steady state of AE amplitude and EP transport can

Fig.10 Time history of fast ion diffusivity from single mode simulations of $n = 4$ RSAE with [panel (**b**)] and without [panel (**a**)] zonal flows in GTC simulation with EP pitch angle scattering
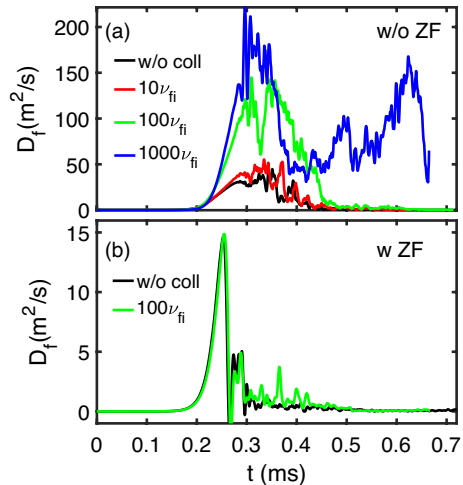
finally be obtained. The results that quasi-steady state of AE turbulence can be maintained with collisions and that AE saturation amplitude increases with the collision frequency are qualitatively consistent with analytical theory (Berk and Breizman 1990) and earlier kinetic-MHD M3D-K (Lang et al. 2010) as well as gyrokinetic GEM simulations (Chen et al. 2013). However, when zonal flows are kept in the GTC simulations, collisional effects on the AE amplitude and EP diffusivity are insignificant, even the collision frequency is amplified by 100 times as shown in Fig. 10(b). The neoclassic transport coefficient of EP can be estimated by the analytic theory (Lin et al. 1995) in the banana regime as $D = 0.2 m^2/s$ for realistic collision frequency $\nu_{fi} \sim 20 s^{-1}$ and in the collisional regime as $D = 15 m^2/s$ for $\nu = 1000 \nu_{fi}$, indicates that the neoclassic EP diffusivity is much smaller than the EP diffusivity induced by the RSAE.

We conclude that the EP collisional effects on the RSAE nonlinear dynamics are negligible for the realistic collision frequency in the DIII-D plasmas. This conclusion is further supported by the estimates of relevant time scales, which show that the RSAE linear growth rate is much larger than the Coulomb collision frequency for the EP. Since resonant beam ions only occupy a small region of the EP phase space, the effective collisional diffusion rate can be amplified using a heuristic factor of $\left(\omega_4/\gamma_4\right)^2$. The effective collisional diffusion rate $\left(\omega_4/\gamma_4\right)^2 \nu_f \sim 0.09 \gamma_4$ is still an order smaller than the RSAE linear growth rate. We note that the fast ion replacement rate (defined as inverse of the fast ion confinement time) is similar to the Coulomb collision frequency. Therefore, the NBI source has negligible effects on the RSAE amplitude and EP transport.

## 5 Nonlinear simulations of multiple toroidal modes

We now perform the nonlinear simulation where multiple toroidal modes $n = [0, 10]$ of the RSAE are kept and interact with each other. As shown in Fig. 11, the normalized electrostatic potentials $\delta\phi$ of the most unstable $n = 4$ RSAE on the q_{min} surface grow to large amplitudes and saturate by the self-generated zonal flows and zonal

structures, which grow with a growth rate of $\gamma \sim 2\gamma_4$. Before the saturation of the $n = 4$ mode at about $0.24ms$, the linearly stable modes such as n = 2 and weakly unstable modes such as $n = 10$ are first generated by numerical coupling of the $n = 4$ mode with linear growth rate $\gamma \sim \gamma_4$. After $0.24ms$, $n = 2$ and $n = 10$ modes are then generated by nonlinear mode coupling of the strongly unstable modes with linear growth rate $\gamma \sim 2\gamma_4$, similar to earlier kinetic-MHD HMGC simulations (Vlad et al. 2018). Moreover, the displaced EPs could also drive more unstable modes in regions that are originally stable. Compared with the single toroidal mode simulations, the saturation amplitude of the $n = 4$ mode is reduced by 20%, while the saturation amplitude of less unstable mode $n = 6$ is reduced by 5 times despite no change in the linear growth rate. At the late nonlinear stage, all mode amplitudes and EP transport drop to a very low level.

The poloidal mode structures from GTC simulation of multiple modes $n = [0,10]$ RSAE are shown in Fig. 12 for the linear phase [panel (a)], at the nonlinear saturation [panel (b)], and the late nonlinear stage [panel (c)]. The corresponding radial profiles of dominant poloidal harmonics are shown in Fig. 13. We find that the most unstable mode $n = 4$ dominates in the linear phase and at the nonlinear saturation, and peaks near the q_{min} flux surface. At the late nonlinear stage, the $n = 4$, $m = 12$ harmonic diminishes near the q_{min} surface. However, a TAE-like mode of $n = 4$ with strong ballooning structure outside the q_{min} flux surface is generated nonlinearly, as shown in Figs.12c and 13c. This TAE is not generated by outward EP transport driven by the RSAE turbulence since the global pressure profiles of all species are fixed in all simulations.

The instantaneous frequency and amplitude for the electrostatic potential $e\delta\phi/T_e$ of the $m = 12$ harmonic near the $q = 3$ flux surface, where the TAE amplitude peaks, are shown in Fig. 14. In linear phase, this harmonic grows exponentially with the linear growth rate and frequency of the $n = 4$ RSAE near the q_{min} surface. Right before the RSAE saturation, the frequency starts to increase, and then splits into two branches ($\sim 86kHz$ TAE and $\sim 142kHz$ EAE) at the nonlinear saturation ($0.23ms$).

Fig. 11 Time histories of perturbed electrostatic potentials $e\delta\phi/T_e$ on the q_{min} flux surface [panel (**a**)] and averaged effective fast ion diffusivity [panel (**b**)] from multiple modes simulation of $n = [0, 10]$
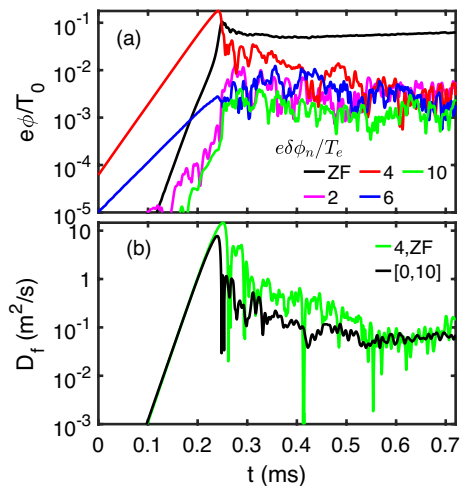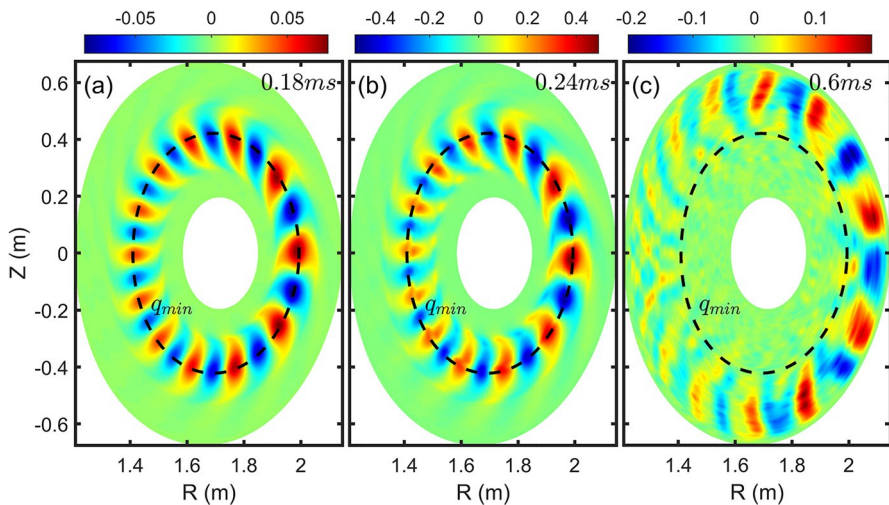
Fig. 12 Poloidal contour plots of perturbed electrostatic potential $e\delta\phi/T_e$ at linear phase [panel (a)], nonlinear saturation [panel (**b**)] and late nonlinear stage [panel (**c**)] from multiple modes simulation of $n = [0, 10]$
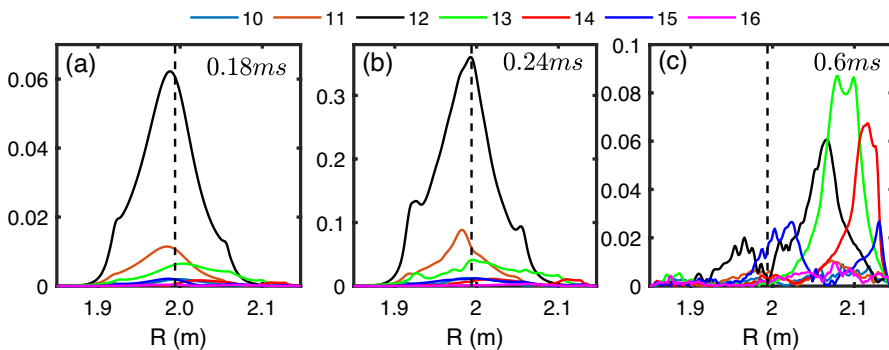
Fig. 13 Radial profiles of poloidal harmonics in linear phase [panel **a**], nonlinear saturation [panel **b**] and late nonlinear stage [panel **c**] from multiple modes simulation of $n = [0, 10]$

During the frequency chirping from RSAE to TAE, the mode growth rate does not change, which does not support the resonant mode coupling. It seems that the nonlinear frequency upshift changes the mode from RSAE to TAE because of frequency and mode structure overlap. The lower frequency TAE branch quickly develops two sidebands ($\sim 65kHz$ and $\sim 90kHz$) accompanied by the drop of mode amplitude due to the rotation of phase space coherent structures (Fasoli et al. 1998). At 0.28ms, the TAE amplitude drops to the lowest level, and the frequency differences of the two TAE sidebands reaches the largest value. Then the two TAE sidebands start to merge accompanied by the increase of the TAE amplitude. After the second frequency bifurcation, a unique TAE persists with a frequency of $\sim 86kHz$. Besides
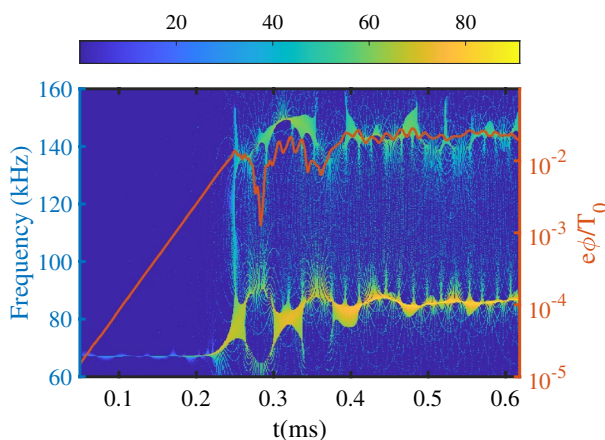
Fig. 14 Time history of frequency spectrum (left) and perturbed electrostatic potential $e\delta\phi/T_e$ of $m = 12$ harmonic near the $q = 3$ flux surface (right)

the TAE, EAE with frequency $\sim 142 kHz$ is also nonlinearly generated after RSAE saturation.

The identification of the TAE and EAE is supported by the Alfven continua (Deng et al. 2012a) as shown in Fig. 15, where the three frequencies for the n = 4 mode observed in the GTC simulation lie in the TAE and EAE gaps.

Unlike the quickly diminished RSAE, the TAE and EAE modes sustain a finite level from $0.4 ms$ to the end of simulation. The TAE and EAE amplitudes are smaller than the RSAE amplitude at the RSAE saturation but larger than that at the late nonlinear stage. The EP diffusivity shown in Fig. 11b exponentially grows with a growth rate of $2\gamma_4$ at linear phase. Compared with EP diffusivity from the single mode simulation of $n = 4$ with zonal flows (green line), the averaged EP diffusivity in the multi-mode simulation (black line) is further reduced to $8 m^2/s$ at the RSAE saturation, but also quickly drops to almost 0 in $0.05 ms$. The EP diffusivity $D_f < 0.2 m^2/s$ near the TAE and EAE mode location is also smaller than the experimental observations.

6 Conclusion and discussion

Using equilibrium geometry and plasma profiles from DIII-D discharge #159,243, nonlinear global gyrokinetic GTC simulations of the RSAE excited by beam ions have been performed to investigate the nonlinear evolution of mode amplitude and associated EP transport. GTC simulations find:

(a) Self-generated zonal flows dominate the RSAE nonlinear saturation by suppressing both mode amplitude and EP transport at the nonlinear saturation.
(b) The flattening of EP profile at the resonance reduces the EP drive and quenches the RSAE after nonlinear saturation.
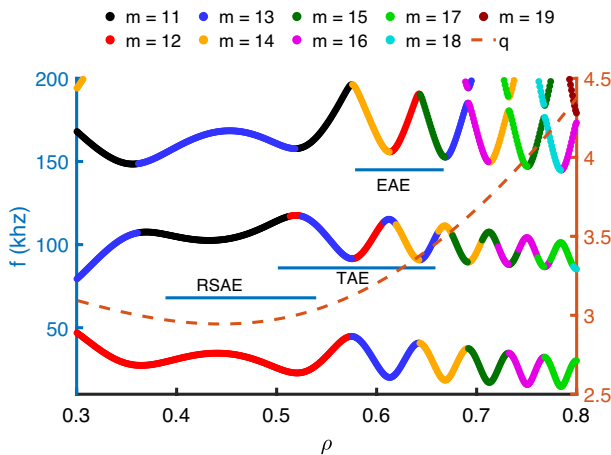
Fig. 15 Alfven continua of $n = 4$. The colored lines represent various poloidal harmonics and the orange dashed line is q profile. Horizontal blue lines represent frequency, radial location and width for RSAE, TAE, and EAE observed in GTC simulation

(c) Effects of EP Coulomb collisions on the RSAE nonlinear dynamics are negligible when using the realistic collision frequency.

(d) Nonlinear interactions between multiple toroidal modes reduce RSAE amplitudes and EP transport.

(e) TAE and EAE in the outer edge can be nonlinearly generated by the RSAE.

(f) Both single mode and multiple modes simulations find a huge initial burst followed by a quickly diminished RSAE amplitude and EP transport, which is inconsistent with experimental observations.

The most important finding from our simulation is that both mode saturation amplitude and associated EP transport are much higher than the experimental observations at the nonlinear saturation, and that diffusivity drops to almost 0 within 0.05 ms after nonlinear saturation. Therefore, nonlinear physics of multiple toroidal modes cannot explain the RSAE amplitude and EP transport measured in the DIII-D experiments. Additional dissipation or background micro-turbulence are believed to affect the AE saturation and EP transport (Zonca et al. 2015; Liu et al. 2022; Bass and Waltz 2010; Duarte et al. 2017; Zeeland et al. 2019; Gorelenkov and Duarte 2021; Biancalani et al. 2021), and integrated simulations incorporating multiple physical processes are required. It should be noted that the present conclusion could also be affected by additional effects, such as slow evolution of the equilibrium profile and EP distribution function, which requires the long time (on the collision time scale) full-f simulation.

Data availability The datasets generated during and/or analysed during the current study are available from the corresponding author on reasonable request.

Declarations

Conflict of interest On behalf of all authors, the corresponding author states that there is no conflict of interest.

References

M.E. Austin, J. Lohr, Electron cyclotron emission radiometer upgrade on the DIII-D tokamak. Rev. Sci. Inst. **74**, 1457 (2003)

E.M. Bass, R.E. Waltz, Gyrokinetic simulations of mesoscale energetic particle-driven alfvénic turbulent transport embedded in microturbulence. Phys. Plasmas **17**, 112319 (2010)

H.L. Berk, B.N. Breizman, Saturation of a single mode driven by an energetic injected beam. III Alfvén wave problem. Phys. Fluids B **2**, 2246 (1990)

H.L. Berk, B.N. Breizman, H. Ye, Scenarios for the nonlinear evolution of alpha-particle-induced Alfvén wave instability. Phys. Rev. Lett. **68**, 3563 (1992)

A. Biancalani et al., Gyrokinetic investigation of Alfvén instabilities in the presence of turbulence. Plasma Phys. Control. Fusion **63**, 065009 (2021)

B.N. Breizman, S.E. Sharapov, Major minority: energetic particles in fusion plasmas. Plasma Phys. Control. Fusion **53**, 054001 (2011)

A.J. Brizard, T.S. Hahm, Foundations of nonlinear gyrokinetic theory. Rev. Mod. Phys. **79**, 421 (2007)

G. Brochard, R. Dumont, H. Lütjens, X. Garbet, T. Nicolas, P. Maget, Nonlinear dynamics of the fishbone-induced alpha transport on ITER. Nucl. Fusion **60**, 126019 (2020)

G. Brochard et al., Verification and validation of linear gyrokinetic and kinetic-MHD simulations for internal kink instability in DIII-D tokamak. Nucl. Fusion **62**, 036021 (2022)

J. Candy, R.E. Waltz, An Eulerian Gyrokinetic-Maxwell Solver. J. Comput. Phys. **186**, 545 (2003)

Y. Chen, S.E. Parker, A Δf particle method for gyrokinetic simulations with kinetic electrons and electromagnetic perturbations. J. Comput. Phys. **189**, 463 (2003)

L. Chen, F. Zonca, Physics of Alfvén waves and energetic particles in burning plasmas. Rev. Mod. Phys. **88**, 015008 (2016)

Y. Chen, T. Munsat, S.E. Parker, W.W. Heidbrink, M.A. Van Zeeland, B.J. Tobias, C.W. Domier, Gyrokinetic simulations of reverse shear Alfvén eigenmodes in DIII-D plasmas. Phys. Plasm. **20**, 012109 (2013)

Y. Chen, G.Y. Fu, C. Collins, S. Taimourzadeh, S.E. Parker, Zonal structure effect on the nonlinear saturation of reverse shear Alfven eigenmodes. Phys. Plasm. **25**, 032304 (2018)

C.Z. Cheng, M.S. Chance, Low-n shear Alfvén spectra in axisymmetric toroidal plasmas. Phys. Fluids **29**, 3695–3701 (1986)

J. Cheng, W. Zhang, Z. Lin, D. Li, C. Dong, J. Cao, Nonlinear co-existence of beta-induced Alfvén eigenmodes and beta-induced Alfvén-acoustic Eigenmodes. Phys Plasm **24**, 092516 (2017)

G.J. Choi, P. Liu, X.S. Wei, J.H. Nicolau, G. Dong, W.L. Zhang, Z. Lin, W.W. Heidbrink, T.S. Hahm, Gyrokinetic simulation of low-frequency Alfvénic modes in DIII-D tokamak. Nucl. Fusion **61**, 066007 (2021)

M.D.J. Cole, A. Biancalani, A. Bottino, R. Kleiber, A. Könies, A. Mishchenko, Toroidal Alfvén Eigenmodes with nonlinear gyrokinetic and fluid hybrid models. Phys. Plasmas **24**, 022508 (2017)

C.S. Collins et al., Observation of critical-gradient behavior in Alfvén-eigenmode-induced fast-ion transport. Phys. Rev. Lett. **116**, 095001 (2016)

W. Deng, Z. Lin, I. Holod, Z. Wang, Y. Xiao, H. Zhang, Linear properties of reversed shear Alfvén eigenmodes in the DIII-D tokamak. Nucl. Fusion **52**, 043006 (2012a)

W. Deng, Z. Lin, I. Holod, Gyrokinetic simulation model for kinetic magnetohydrodynamic processes in magnetized plasmas. Nucl. Fusion **52**, 023005 (2012b)

G. Dong, J. Bao, A. Bhattacharjee, A. Brizard, Z. Lin, P. Porazik, Gyrokinetic particle simulations of the effects of compressional magnetic perturbations on Drift-Alfvenic instabilities in tokamaks. Phys. Plas. **24**, 081205 (2017)

V.N. Duarte, H.L. Berk, N.N. Gorelenkov, W.W. Heidbrink, G.J. Kramer, R. Nazikian, D.C. Pace, M. Podestà, B.J. Tobias, M.A. Van Zeeland, Prediction of nonlinear evolution character of energetic-particle-driven instabilities. Nucl. Fusion **57**, 054001 (2017)

A. Fasoli, B.N. Breizman, D. Borba, R.F. Heeter, M.S. Pekker, S.E. Sharapov, Nonlinear splitting of fast particle driven waves in a plasma: observation and theory. Phys. Rev. Lett. **81**, 5564 (1998)

A. Fasoli et al., Chapter 5: physics of energetic Ions. Nucl. Fusion **47**, S264 (2007)

G.Y. Fu, W. Park, Nonlinear hybrid simulation of the toroidicity-induced Alfvén Eigenmode. Phys. Rev. Lett. **74**, 1594 (1995)

N.N. Gorelenkov, V.N. Duarte, Microturbulence-mediated route for energetic ion transport and Alfvénic mode amplitude oscillations in tokamaks. Phys. Lett. A **386**, 126944 (2021)

N.N. Gorelenkov, S.D. Pinches, K. Toi, Energetic particle physics in fusion research in preparation for burning plasma experiments. Nucl. Fusion **54**, 125001 (2014)

W.W. Heidbrink, Basic physics of Alfvén instabilities driven by energetic particles in toroidally confined plasmas. Phys. Plasmas **15**, 055501 (2008)

W.W. Heidbrink, R.B. White, Mechanisms of energetic-particle transport in magnetically confined plasmas. Phys. Plasmas **27**, 030901 (2020)

W.W. Heidbrink, J.M. Park, M. Murakami, C.C. Petty, C. Holcomb, M.A. Van Zeeland, Evidence for fast-ion transport by microturbulence. Phys. Rev. Lett. **103**, 175001 (2009)

W.W. Heidbrink, C.S. Collins, M. Podestà, G.J. Kramer, D.C. Pace, C.C. Petty, L. Stagner, M.A. Van Zeeland, R.B. White, Y.B. Zhu, Fast-Ion transport by Alfvén eigenmodes above a critical gradient threshold. Phys. Plasmas **24**, 056109 (2017)

H. Hezaveh, Y. Todo, Z. Qu, B. Breizman, M. Hole, Simulation of convective transport during frequency chirping of a TAE using the MEGA code. Nucl. Fusion **62**, 036025 (2022)

F.L. Hinton, R.D. Hazeltine, Theory of plasma transport in toroidal confinement systems. Rev. Mod. Phys. **48**, 239 (1976)

W. Horton, Drift waves and transport. Rev. Mod. Phys. **71**, 735 (1999)

S. Jolliet, A. Bottino, P. Angelino, R. Hatzky, T.M. Tran, B.F. Mcmillan, O. Sauter, K. Appert, Y. Idomura, L. Villard, A global collisionless PIC code in magnetic coordinates. Comp. Phys. Communicat. **177**, 409 (2007)

J. Lang, G.-Y. Fu, Y. Chen, Nonlinear simulation of toroidal Alfvén eigenmode with source and sink. Phys. Plasmas **17**, 042309 (2010)

P. Lauber, Super-thermal particles in hot plasmas—kinetic models, numerical solution strategies, and comparison to tokamak experiments. Phys. Rep. **533**, 33 (2013)

Z. Lin, W.M. Tang, W.W. Lee, Gyrokinetic particle simulation of neoclassical transport. Phys. Plasmas **2**, 14 (1995)

Z. Lin, T.S. Hahm, W.W. Lee, W.M. Tang, R.B. White, Turbulent transport reduction by zonal flows: massively parallel simulations. Science **281**, 1835 (1998)

Z. Lin, S. Ethier, T.S. Hahm, W.M. Tang, Size scaling of turbulent transport in magnetically confined plasmas. Phys. Rev. Lett. **88**, 195004 (2002)

P. Liu, X. Wei, Z. Lin, G. Brochard, G.J. Choi, W.W. Heidbrink, J.H. Nicolau, G.R. McKee, Regulation of Alfvén eigenmodes by microturbulence in fusion plasmas. Phys. Rev. Lett. **128**, 185001 (2022)

J. McClenaghan, Z. Lin, I. Holod, W. Deng, Z. Wang, Verification of gyrokinetic particle simulation of current-driven instability in fusion plasmas i internal kink mode. Phys. Plasmas **21**, 122519 (2014)

A. Mishchenko, A. Könies, R. Kleiber, M. Cole, Pullback transformation in gyrokinetic electromagnetic simulations. Phys. Plasmas **21**, 092110 (2014)

J.H. Nicolau, G. Choi, J. Fu, P. Liu, X. Wei, Z. Lin, Global Gyrokinetic simulation with kinetic electron for collisionless damping of zonal flow in stellarators. Nucl. Fusion **61**, 126041 (2021)

S.E. Parker, W.W. Lee, A fully nonlinear characteristic method for gyrokinetic simulation. Phys. Fluids B **5**, 77 (1993)

S.D. Pinches et al., The HAGIS self-consistent nonlinear wave-particle interaction model. Comp. Phys. Communicat. **111**, 133 (1998)

D.A. Spong, B.A. Carreras, C.L. Hedrick, Nonlinear evolution of the toroidal Alfvén instability using a gyro-fluid model. Phys. Plasmas **1**, 1503 (1994)

D.A. Spong, E.M. Bass, W. Deng, W.W. Heidbrink, Z. Lin, B. Tobias, M.A. Van Zeeland, M.E. Austin, C.W. Domier, N.C. Luhmann, Verification and Validation of linear gyrokinetic simulation of Alfvén eigenmodes in the DIII-D tokamak. Phys. Plasmas **19**, 082511 (2012)

S. Taimourzadeh et al., Verification and validation of integrated simulation of energetic particles in fusion plasmas. Nucl. Fusion **59**, 066006 (2019)

B. Tobias et al., Commissioning of electron cyclotron emission imaging instrument on the DIII-D tokamak and first data. Rev. Sci. Inst. **81**, 10D928 (2010)

Y. Todo, Introduction to the Interaction between energetic particles and Alfven eigenmodes in toroidal plasmas. Rev. Mod. Plasma Phys. **3**, 1 (2019)

Y. Todo, T. Sato, Linear and nonlinear particle-magnetohydrodynamic simulations of the toroidal Alfvén eigenmode. Phys. Plasmas **5**, 1321 (1998)

Y. Todo, H.L. Berk, B.N. Breizman, Simulation of intermittent beam ion loss in a tokamak fusion test reactor experiment. Phys. Plasmas **10**, 2888 (2003)

Y. Todo, H.L. Berk, B.N. Breizman, Nonlinear magnetohydrodynamic effects on Alfvén eigenmode evolution and zonal flow generation. Nucl. Fusion **50**, 084016 (2010)

M.A. Van Zeeland et al., Alfvén eigenmodes and fast ion transport in negative triangularity DIII-D plasmas. Nucl. Fusion **59**, 086028 (2019)

J. Varela, D.A. Spong, L. Garcia, Analysis of Alfvén eigenmode destabilization by energetic particles in large helical device using a landau-closure model. Nucl. Fusion **57**, 046018 (2017)

G. Vlad, S. Briguglio, G. Fogaccia, V. Fusco, C. Di Troia, E. Giovannozzi, X. Wang, F. Zonca, Single- n versus multiple- n simulations of Alfvénic modes. Nucl. Fusion **58**, 082020 (2018)

Z. Wang, Z. Lin, I. Holod, W.W. Heidbrink, B. Tobias, M. Van Zeeland, M.E. Austin, Radial localization of toroidicity-induced alfvén eigenmodes. Phys. Rev. Lett. **111**, 145003 (2013)

H.Y. Wang, I. Holod, Z. Lin, J. Bao, J.Y. Fu, P.F. Liu, J.H. Nicolau, D. Spong, Y. Xiao, Global gyrokinetic particle simulations of microturbulence in W7-X and LHD stellarators. Phys. Plasmas **27**, 082305 (2020)

X.Q. Wang et al., Nonlinear simulations of energetic particle-driven instabilities interacting with Alfvén continuum during frequency chirping. Plasma Phys. Control. Fusion **63**, 015004 (2021)

H. Wang, P. Liu, Z. Lin, W. Zhang, Linear gyrokinetic simulations of reversed shear Alfvén eigenmodes and ion temperature gradient modes in DIII-D tokamak. Plasma Sci. Technol. **23**, 015101 (2021)

R.B. White, *The theory of toroidally confined plasmas* (Published By Imperial College Press And Distributed By World Scientific Publishing Co, USK, 2006)

Y. Xiao, Z. Lin, Turbulent transport of trapped-electron modes in collisionless plasmas. Phys. Rev. Lett. **103**, 085004 (2009)

W. Zhang, Z. Lin, L. Chen, Transport of energetic particles by microturbulence in magnetized plasmas. Phys. Rev. Lett. **101**, 095001 (2008)

H.S. Zhang, Z. Lin, I. Holod, Nonlinear frequency oscillation of Alfvén eigenmodes in fusion plasmas. Phys. Rev. Lett. **109**, 025001 (2012)

H.S. Zhang, Z. Lin, W. Deng, I. Holod, Z.X. Wang, Y. Xiao, W.L. Zhang, Nonlinear dynamics of beta-induced Alfvén eigenmode in tokamak. Phys Plasmas **20**, 012510 (2013)

F. Zonca, L. Chen, Theory on excitations of drift Alfvén waves by energetic particles. II the general fishbone-like dispersion relation. Phys. Plasmas 21, 072121 (2014)

F. Zonca, L. Chen, S. Briguglio, G. Fogaccia, G. Vlad, X. Wang, Nonlinear dynamics of phase space zonal structures and energetic particle physics in fusion plasmas. New J. Phys. **17**, 013052 (2015)